Journal of Applied Polymer Science

Fabrication of Tiron-doped polypyrrole/MWCNT composite electrodes with high mass loading and enhanced performance for supercapacitors

Kaiyuan Shi,[1] Xin Pang,[2] Igor Zhitomirsky[1]
[1]Department of Materials Science and Engineering, McMaster University, Hamilton Ontario, Canada L8S 4L7
[2]CanmetMATERIALS, Natural Resources Canada, Hamilton Ontario, Canada L8P 0A5
Correspondence to: I. Zhitomirsky (E-mail: zhitom@mcmaster.ca)

ABSTRACT: In this study, the aromatic sulfonate compound Tiron with high charge to mass ratio is used as an anionic dopant for synthesis of polypyrrole (PPy). The fabricated PPy is investigated for electrochemical supercapacitor (ES) application. Testing results show that Tiron allows reduced PPy agglomeration, smaller particle size and improved charge storage properties of PPy. High capacitance and improved capacitive retention at high scan rates are achieved by the fabrication of PPy/multiwalled carbon nanotube (MWCNT) composite electrode using safranin (SAF) as a co-dispersant. The Tiron-doped PPy electrode shows the highest capacitance of 7.8 F cm^{-2} with a mass of 27 mg cm^{-2}. The Tiron-doped PPy/MWCNT composite electrode shows good capacitance retention with a capacitance of 1.0 F cm^{-2} at the scan rate of 100 mV s^{-1}. Symmetric supercapacitor cells are fabricated using PPy based active materials. An energy density of 0.36 mWh cm^{-2} is achieved. The energy/power density and capacitance retention of the Tiron-doped PPy/MWCNT ES is significantly improved in comparison with PPy-based ES, prepared without Tiron or MWCNT. The Tiron-doped PPy/MWCNT symmetric supercapacitor presents good cycling performance with 91.4% capacitance retention after 1000 charge–discharge cycles. The PPy/MWCNT composites, prepared using Tiron and SAF co-dispersant, are promising electrodes for ES.
 J. Appl. Polym. Sci. **2015**, *132*, 42376.

KEYWORDS: adsorption; batteries and fuel cells; colloids; conducting polymers; electrochemistry

Received 14 December 2014; accepted 14 April 2015
DOI: 10.1002/app.42376

INTRODUCTION

The growing interest in the application of polypyrrole (PPy) for electrodes of electrochemical supercapacitors (ES) is attributed to the relatively high specific capacitance (SC), low cost, high electrical conductivity, advanced chemical and mechanical properties of PPy.[1,2] Many investigations[3–5] have been conducted with the objective to utilize the high theoretical SC of PPy (620 F g^{-1}) in ES. The high SC of PPy results from redox reactions, which allow charge storage in the bulk of the electrode material. However, poor cycling stability of PPy limited its application in ES. It is found that swelling and shrinking occurred during anion exchange between PPy and electrolyte, which resulted in the increased impedance, gradual adhesion loss and poor cycling behavior of PPy electrode.[6] The increase of PPy mass loading deteriorated the cyclic stability and decreased the electrode SC.[6]

Electropolymerization and chemical polymerization are attractive methods for the preparation of PPy for ES application. However, it is difficult to achieve high active material loading of the electrode using electrochemical synthesis.[7,8] For practical applications of ES, it is always desirable to increase the active material loading and achieve high SC at high charge–discharge rates.[9,10] Chemical polymerization of PPy offers advantages for the fabrication of PPy-based ES with high mass loadings. The use of anionic dopants for chemical synthesis of PPy could improve its charge storage properties and cycle performance.[11–13] It has been shown that with the variation of the dopant anion, the conductivity of the PPy can differ by three orders of magnitude.[14] Beside affecting conductivity, dopants could also improve the thermal stability,[15] surface morphology[16,17] and mechanical strength[18] of PPy. Considering these facts, it is of great interest to achieve high electrochemical activity of PPy for ES application using dopants. The interest in application of Tiron as an anionic dopant is attributed to its relatively high charge to mass ratio, compared to other aromatic sulfonate dopants. It is in this regard that the investigation of electrochemically prepared PPy, containing aromatic sulfonate dopants, showed that film conductivity increased with increasing charge to mass ratio of the dopant molecules.[19]

Recently, a great advancement has been achieved by using carbon nanotube (CNT) to improve the rate capability of PPy-based electrode because of their superior electrical conductivity and high specific surface area.[9,20–22] However, both CNT and PPy are prone to agglomeration in the fabrication process. As a result, the pores in the electrodes are partially inaccessible to the electrolyte. Therefore, the development of new processing strategies, utilizing new dispersants, is scientifically attractive to the fabrication of advanced PPy-based ES electrode.

In this study, PPy was chemically synthesized using Tiron as an anionic dopant for the fabrication of electrodes for ES. The obtained Tiron-doped PPy showed high electrochemical activity, which allowed improved charge storage for ES application. Additionally, a facile route for the fabrication of PPy nanocomposites with multiwalled carbon nanotube (MWCNT) has been developed using safranin (SAF) as a co-dispersant for PPy and MWCNT. The obtained Tiron-doped PPy/MWCNT composite has shown improved capacitance retention at high scan rates, compared to pure PPy. The results open new processing method for the fabrication of advanced PPy/MWCNT composite electrode by colloidal nanotechnology.

EXPERIMENTAL

Materials

Pyrrole (Py), 4,5-dihydroxy-1,3-benzenedisulfonic acid disodium salt (Tiron), ammonium persulfate (APS) and SAF were purchased from Sigma-Aldrich. MWCNT was provided by Arkema. Py was stored in a refrigerator at 4°C before use. All chemicals were used as received without any further purification. Ni foam current collector with a volumetric porosity of 95% was supplied by Vale company.

Synthesis of Tiron-doped PPy

PPy was prepared by chemical polymerization reaction with APS as the oxidant at 0°C. 4.98 g Tiron (15 mmol) was dissolved in 50 mL de-ionized water, followed by injecting 1.04 mL (15 mmol) pyrrole under a vigorous magnetic stirring for 30 min in an ice bath. Then 50 mL of 0.3 mol L^{-1} APS solution was slowly added to the above solution. The resultant mixture was subsequently allowed to react for 20 h. To study the effect of Tiron, PPy polymer was also prepared using the same concentration of Py and APS but without Tiron. The precipitated PPy solids were filtered and washed by 2 L de-ionized water and 500 mL ethanol. The obtained powders were dried at 70°C for 12 h.

Tiron-Doped PPy/MWCNT Slurry Preparation

0.34 g of as-prepared Tiron-doped PPy was put into 400 mL solution, containing 0.5 g L^{-1} SAF, and sonicated in an ultrasonic bath for 20 min in order to form a homogeneous colloidal solution. 0.06 g MWCNT was then added and further ultrasonicated for 1 hr. A stable Tiron-doped PPy/MWCNT suspension was obtained. A vacuum filtration process was applied to fabricate homogeneous Tiron-doped PPy/MWCNT slurry. Excess SAF in the mixture was removed by the filtration system until the DI-water dropped from the funnel was colorless. The filtration system consisted of four components, namely a set of Buchner funnel with sand core (45 mm in diameter), a suction flask, a membrane filter (Nuclepore Whatman, 1 μm pore size) and a water circulation vacuum pump.

Characterization

The morphologies of prepared products were investigated using a JEOL JSM-7000F scanning electron microscope (SEM). The sedimentation tests were carried out using 1 g L^{-1} MWCNT and 1 g L^{-1} Tiron-doped PPy with and without SAF (0.5 g L^{-1}) dispersant. The obtained suspension was filtered for the Fourier transform infrared spectroscopy (FTIR) analysis. FTIR studies were performed on Bio-Rad FTS-40 instrument.

The working electrodes were fabricated using dispersed PPy based active materials without any binder. A small amount of de-ionized water was added into the mixture to produce a homogeneous paste, which was impregnated in Ni foam substrates with an area of 1 cm^2 to form electrodes with different mass loadings. The impregnated Ni foam was roller pressed to ~20% of the initial thickness. Electrochemical studies were performed using a potentiostat (PARSTAT 2273, Princeton Applied Research). The counter electrode was a platinum gauze, and the reference electrode was a standard calomel electrode (SCE). Capacitive behavior and electrochemical impedance were investigated in 0.5*M* Na_2SO_4 aqueous solutions. Cyclic voltammetry (CV) studies were performed within a potential range of −0.5 to +0.4 V versus SCE at scan rates of 0.5–100 mV s^{-1}. The total capacitance $C = Q/\Delta V$ was calculated using half the integrated area of the CV curve to obtain the charge Q, and subsequently dividing the charge Q by the width of the potential window ΔV. The mass-normalized specific capacitance $C_m = C/M$ (M-sample mass) and area-normalized specific capacitance $C_s = C/S$ (S-sample area) were calculated from the CV data. The alternating current (AC) measurements of complex impedance $Z^* = Z' - iZ''$ were conducted in the frequency range of 10 mHz to 100 kHz and the amplitude of the AC signal was 5 mV. The impedance data were also analyzed using the method described in Ref. 23. In this method, the complex capacitance $C^* = C' - iC''$ was calculated from the impedance data as $C' = Z''/\omega|Z|^2$ and $C'' = Z'/\omega|Z|^2$, where $\omega = 2\pi f$ (f—frequency).

The coin cells were formed using coin cell cases (CR2032 type, MTI Corporation). The symmetric cell contained two similar electrodes, separated with a porous membrane. The cells were sealed using a hydraulic crimping machine (MSK-110, MTI Corporation). The capacitance of the supercapacitor cell (C_c) was calculated using the equation $C_c = I\Delta t/m\ \Delta V$, where I is the constant discharge current, Δt is the discharge time, m is the total mass of active materials in both electrodes, and ΔV is the voltage drop upon discharging.

RESULTS AND DISCUSSION

Figure 1(A,B) show the SEM images of PPy prepared without Tiron. The morphology exhibits an agglomerated cauliflower-like structure, consisting of many spherical particles. The mechanism of chemical polymerization of PPy in the presence of dopants and oxidants was discussed in the literature.[11,24] Upon the addition of oxidant solution to the monomer solution, each neutral pyrrole molecule is oxidized by APS and yields a free cationic radical, which then combines with another radical to

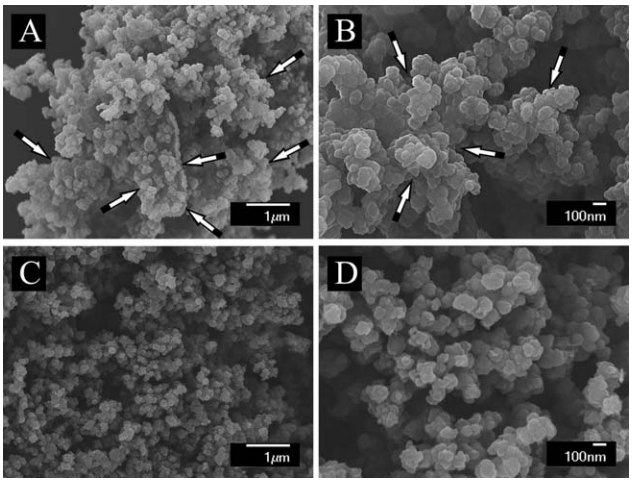

Figure 1. SEM images at different magnifications of (A, B) PPy prepared without Tiron, arrows show agglomerates of particles; and (C, D) Tiron-doped PPy.

form a dimer. The dimers are further combined with other free cationic radicals to form trimers and so on, finally resulting in chains of positively charged PPy units. The anionic dopants are incorporated into the polymer matrix and compensate the positive charge of PPy.[25,26] Figure 1(C,D) show that the Tiron-doped PPy has a fine structure. They demonstrated that Tiron could reduce the agglomeration of PPy particles.

The sedimentation test showed that as-prepared PPy was not stable in the aqueous suspension. It is suggested that fine PPy particles in suspension formed agglomerates, which promoted PPy precipitation. It is known that particle agglomeration results in reduced surface area, which deteriorates the capacitance behavior of active materials.[27] In this study, we found that Tiron-doped PPy and MWCNT can be well dispersed using SAF as a co-dispersant. Figure 2(A) shows the molecular structure of cationic polyaromatic SAF, which includes two methyl groups and two NH_2 groups. SAF offers advantages for dispersion, compared to long chain surfactants, which are widely used for the dispersion of carbon nanotubes.[28] In general, surfactants have both polar (hydrophilic) and nonpolar (hydrophobic) moieties.[29,30] The hydrophilic head of adsorbed surfactant is directed toward the bulk water, and the hydrophobic tail provides adsorption on the carbon nanotube surface via hydrophobic interactions. The adsorbed long chain surfactants create insulating layers on the carbon nanotube surface, which reduce the efficiency of carbon nanotubes for application as conductive additives in the composites. Due to the weak hydrophobic interactions, relatively large concentrations of surfactants are required for the carbon nanotube dispersion. It was found that surfactants can provide dispersion at relatively low carbon nanotube concentrations.[31–33] It is in this regard that the smaller size of SAF molecules is beneficial for dispersion of MWCNT. The adsorption of SAF on both PPy and MWCNT involves the π–π interactions. The positive charge of adsorbed SAF results in electrostatic repulsion of PPy and MWCNT and improves dispersion of both materials. Figure 2(B) is the scheme of Tiron-doped PPy/MWCNT suspension fabrication. The pristine Tiron-doped PPy and MWCNT show a very quick

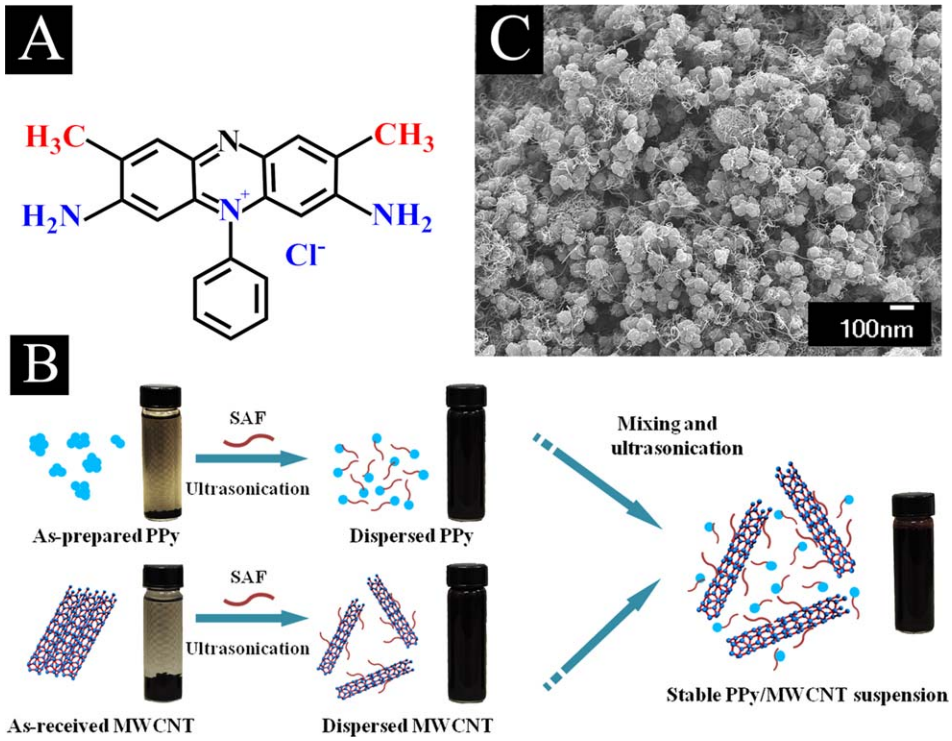

Figure 2. (A) Chemical structure of SAF, (B) Scheme of Tiron-doped PPy/MWCNT suspension fabrication and (C) SEM image of Tiron-doped PPy/MWCNT composite obtained from a mixed Tiron-doped PPy/MWCNT suspension. [Color figure can be viewed in the online issue, which is available at wileyonlinelibrary.com.]

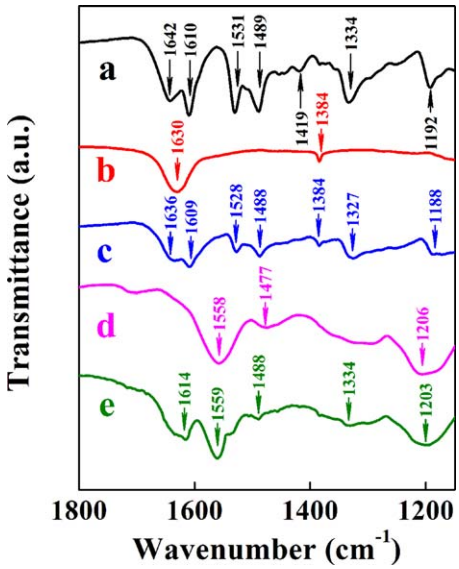

Figure 3. FTIR for (a) SAF, (b) pristine MWCNT, (c) SAF dispersed MWCNT (d) Tiron-doped PPy, (e) SAF dispersed Tiron-doped PPy. [Color figure can be viewed in the online issue, which is available at wileyonlinelibrary.com.]

precipitation after 1–2 h. After adding SAF into MWCNT and Tiron-doped PPy, the suspensions showed no precipitation after two weeks. Mixed Tiron-doped PPy and MWCNT suspensions were homogenous and stable. SEM image [Figure 2(C)] showed the Tiron-doped PPy/MWCNT composite fabricated by mixing of the suspensions, followed by a vacuum filtration process. The results indicated that MWCNTs were well dispersed in the PPy matrix. Good dispersion of MWCNTs allowed the fabrication of PPy electrode with improved capacitive performance.

The MWCNT and Tiron-doped PPy were analyzed by FTIR [Figure 3(a–e)]. The FTIR spectrum of SAF [Figure 3(a)] was in agreement with literature data.[34,35] The C═C stretching of the benzene rings contributed to the bands at 1531 and 1489 cm^{-1}. The absorption at 1610 cm^{-1} is attributed to the NH_2— asymmetric deformation. The C═N stretching appears at the 1642 and 1334 cm^{-1}. The FTIR spectrum of MWCNT [Figure 3(b)] showed the absorption at 1630–1635 cm^{-1}, related to the C═O stretching of quinone groups of MWCNT. The bending vibration of the —OH group contributed to the band at 1384 cm^{-1}.[36] The peaks at 1558 and 1477 cm^{-1} in Figure 3(d) are assigned to C—N and C—C asymmetric and symmetric ring-stretching of PPy, respectively. In addition, strong peak near 1206 cm^{-1} is attributed to symmetric and asymmetric stretching vibration of SO_3Na group of Tiron dopant.[37] The IR absorption is associated with changes in the conjugated structure of conductive polymer.[38,39] Rodrıguez *et al.*[40] suggested that it is depended on the oxidation-state and charge carriers of the PPy chains. In comparison with the spectra of pristine MWCNT and Tiron-doped PPy, the spectra of dispersed materials [Figure 3(c,e)] showed additional adsorptions at 1609, 1528, 1488, 1327 cm^{-1} for dispersed MWCNT and at 1614 and 1334 cm^{-1} for dispersed Tiron-doped PPy. Taking into account that similar absorptions were observed in the spectrum of SAF, it was concluded that the dispersed MWCNT and Tiron-doped PPy contained adsorbed SAF.

Figure 4(A) shows typical cyclic voltammograms for the different electrodes. The incorporation of Tiron into the PPy matrix resulted in improved capacitive behavior, as indicated by the differences in current between undoped PPy [Figure 4A(a)] and Tiron-doped PPy [Figure 4A(b)]. The cyclic voltammogram area for Tiron-doped PPy is significantly larger than that for PPy without Tiron, indicating a higher capacitance of the doped material. While the Tiron-doped sample with a low mass loading showed a nearly box-shaped cyclic voltammogram, deviation from the ideal box-shaped cyclic voltammogram was observed when the mass loading was increased to 27 mg cm^{-2} [Figure 4A(c)]. The CV curve of SAF dispersed composite electrode with the same mass [Figure 4A(d)] has a nearly box shape, suggesting the capacitive performance was improved by utilization of MWCNT and co-dispersant.

Measurements of C_m and C_s at different conditions are important for understanding the electrochemical behavior of PPy electrodes and optimizing their performance. As shown in Figure 4(B), the C_m calculated from the CV data for 14 mg cm^{-2} undoped PPy was only 174 F g^{-1} at a scan rate of 0.5 mV s^{-1}. The Tiron-doped PPy, prepared from 15 mmol pyrrole solutions in presence of 15 mmol Tiron and 15 mmol APS showed a capacitance of 309 F g^{-1}. For comparison, the electrodes of the same mass, prepared from 15 mM pyrrole solutions in presence of 15 mmol KCl and 15 mmol APS showed a capacitance of 217 F g^{-1}. The increase in the scan rate and mass loading resulted in a decreasing C_m. Recent studies[41] showed that high C_m values of electrode materials do not necessarily indicate good capacitive behavior due to the strong dependence of C_m on the electrode mass. It was shown that reporting gravimetric characteristics (such as C_m) alone cannot provide a realistic picture of material performance, especially at high material loadings. Therefore, C_s data for the composite electrode were presented in Figure 4(C). The Tiron-doped PPy showed an increased C_s of 4.4 F cm^{-2} at a mass loading of 14 mg cm^{-2} [Figure 4C(b)], compared with 2.8 F cm^{-2} for the undoped PPy [Figure 4C(a)]. With an increase of mass loading to 28 mg cm^{-2}, Tiron-doped PPy showed a C_s of 6.5 F cm^{-2}. However, the C_s was only 0.3 F cm^{-2} at a scan rate of 100 mV s^{--1} [Figure 4C(c)]. The SAF dispersed composite electrode showed improved capacitance retention at high scan rates. A C_s of 1.1 F cm^{-2} was obtained at a scan rate of 100 mV s^{-1} [Figure 4C(d)]. It is known that MWCNT has relatively low SC($\sim$ 20 F g^{-1})[42,43] and Tiron-doped PPy showed SC of 309 F g^{-1}. Therefore, the contribution of CNT to the capacitance of the composite electrode is relatively small. The impedance measurements [Figure 4(D)] showed that the undoped PPy has a large electrode resistance Z' compared to the Tiron-doped PPy. The increase in the mass loading enlarged the width of the high frequency semicircle. Compared with pure PPy, the Z' was reduced for Tiron-doped PPy/MWCNT composite.

The mechanism of decrease of electrode resistance of PPy by the dopant is proposed in Refs. 44,45. The charge introduced

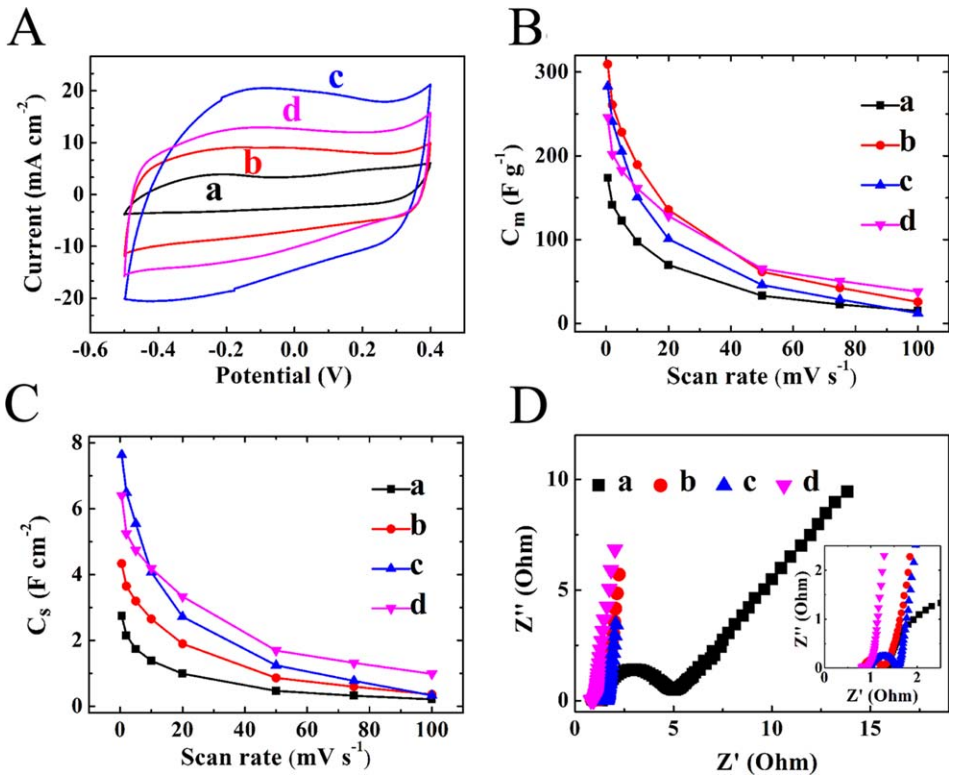

Figure 4. (A) CV data at a scan rate of 2 mV s^{-1}, (B) C_m and (C) C_s obtained from the CV data versus scan rate and (D) Nyquist plot of Z^* (inset shows high frequency range) for (a) PPy without Tiron with a mass of 14 mg cm^{-2}; (b)Tiron-doped PPy with a mass of 14 mg cm^{-2}; (c) Tiron-doped PPy with a mass of 27 mg cm^{-2}; (d) Tiron-doped PPy/MWCNT composite with a mass of 27 mg cm^{-2}. [Color figure can be viewed in the online issue, which is available at wileyonlinelibrary.com.]

upon doping process of PPy stores in the form of polarons and bipolarons. The formation of polarons and/or bipolarons induces the change in the phase of the double bonds and the creation of a domain with a quinoid sequence of double bonds, responsible for electrical conduction in the PPy chain.[44]

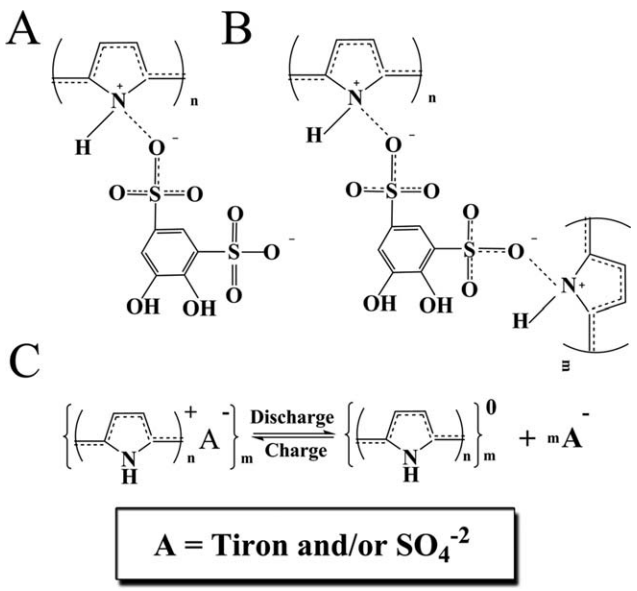

Figure 5. (A, B) Tiron doping of PPy: (A) in the same chain and (B) in different polymer chains, (C) the charge–discharge mechanism of Tiron-doped PPy.

The sulfonic groups of Tiron can be involved in the doping of one PPy molecule [Figure 5(A)] or two different polymer chains [Figure 5(B)]. In the latter case the dopant can enhance the interchain mobility of charge carriers and improve the electrical conductivity of the PPy material.[46] The charge and discharge mechanism of Tiron-doped PPy electrode in Na_2SO_4 as the electrolyte is shown in Figure 5(C). During the discharge process, the PPy is reduced (de-doped) to its neutral state by unchaining the incorporated anions A^-. For the undoped PPy, the released ions A^- is SO_4^{2-}. Tiron allows the improvement of charge storage of PPy because the dopant anions can be released during the reduction.[47,48] The anions could migrate back to the polymers during the charging process.

The analysis of capacitive behavior from EIS data showed higher capacitance of Tiron-doped PPy compared with undoped PPy [Figure 6(A,B)]. It was found that C_s' are 0.6 and 2.5 F cm^{-2} at frequency of 0.01 Hz for undoped PPy and Tiron-doped PPy with a mass of 14 mg cm^{-2}, respectively [Figure 6(A)]. The improved capacitance behavior might be mainly ascribed to the smaller particle sizes and lower impedance of Tiron-doped PPy. An increase in the mass loading resulted in a higher C_s' at the low frequency; however, the capacitance decreased sharply with the increase of frequency. The corresponding C_s'' curves [Figure 6(B)] showed typical relaxation maxima. With an increasing

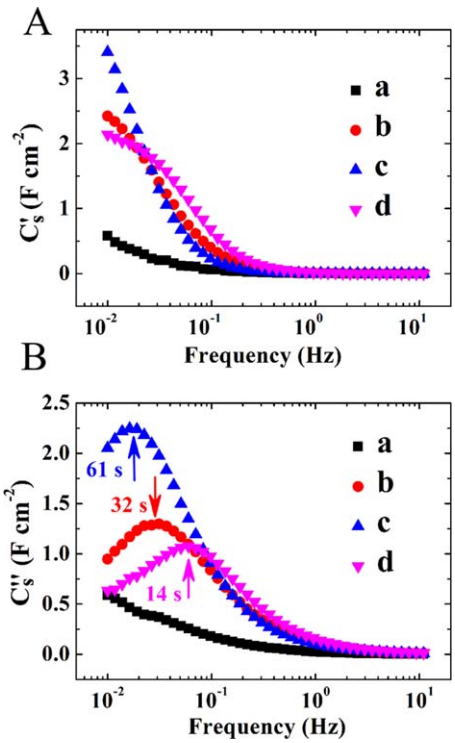

Figure 6. (A) C_s' and (B) C_s'' obtained from the impedance data versus frequency for (a) undoped PPy with a mass of 14 mg cm^{-2}; (b) Tiron-doped PPy with a mass of 14 mg cm^{-2}; (c) Tiron-doped PPy with a mass of 27 mg cm^{-2}; and (d) Tiron-doped PPy/MWCNT composite with a mass of 27 mg cm^{-2}. [Color figure can be viewed in the online issue, which is available at wileyonlinelibrary.com.]

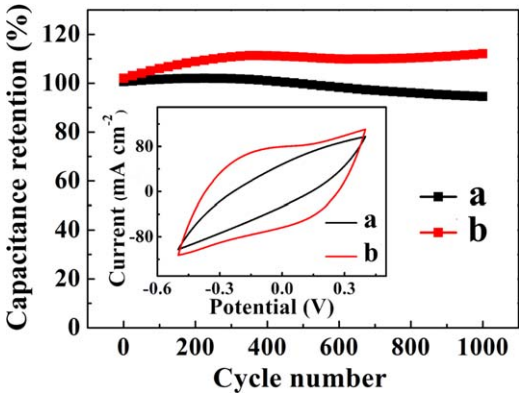

Figure 7. Capacitance retention as a function of cycle number, inset shows corresponding CVs after 1000 cycles at a scan rate of 50 mV s^{-1} for (a) Tiron-doped PPy and (b) Tiron-doped PPy/MWCNT composite with a mass of 27 mg cm^{-2}. [Color figure can be viewed in the online issue, which is available at wileyonlinelibrary.com.]

mass loading, the relaxation frequencies shifted to lower frequencies. The relaxation times $\tau = 1/f_m$, related to the C_s'' maxima, were found to be 32, 61, and 14 s for 14 mg cm^{-2} Tiron-doped PPy, 27 mg cm^{-2} Tiron-doped PPy and 27 mg cm^{-2} Tiron-doped PPy–MWCNT composite, respectively. The results of C^* analysis further confirmed that the Tiron-doped electrodes exhibited improved capacitive behavior compared to the undoped PPy. SAF dispersed PPy/MWCNT composite preserved the capacitance behavior at higher frequencies. This phenomenon could be explained by the charge storage nature of the bulk pseudo-capacitive material, which is controlled by both diffusion process and charge transfer process.[49–52] Diffusion limitations at high scan rates or high frequencies will result in poor electrolyte access to the bulk of composite PPy electrode. Furthermore, PPy has difficulty in transferring Faradaic charges compared with the PPy/MWCNT composite, because the pure PPy has a higher resistance than the PPy/MWCNT composite, as shown in Figure 4(D). The difficulty of PPy to transfer charges causes its pseudo-capacitive properties to become negligible at high scan rates.[53] The decrease of differential capacitance, derived from the impedance data, with the increasing frequency correlates with the decrease in integral capacitance with the increasing scan rate, as shown in Figure 4(B,C), respectively.

The three-electrode cycling performance of Tiron-doped PPy and SAF dispersed composite was shown in Figure 7. The capacitance slightly increased during the initial cycles. After 400 cycles, no obvious capacity fading was observed for any of the electrodes. The capacitance retentions after 1000 cycles are 94% and 112% for Tiron-doped PPy and PPy/MWCNT composite electrode respectively. The CV of Tiron-doped PPy/MWCNT remains a quasi-rectangular shape at a scan rate of 50 mV s^{-1} after 1000 cycles (Figure 7, inset). Figure 8 shows the microstructures of the Tiron-doped PPy after 1000 cycles. The SEM results indicate that cycling resulted in increasing porosity and fibrous microstructure, which may result in the increase of capacitance during the first 250 cycles.

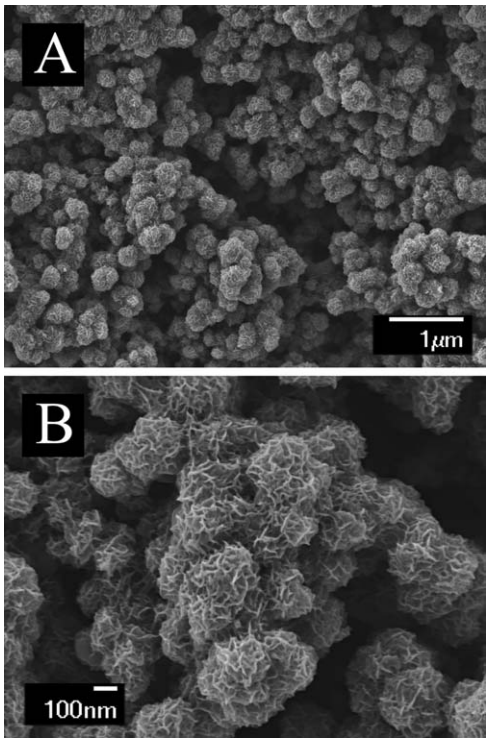

Figure 8. SEM images of Tiron-doped PPy after 1000 CV cycles at different magnifications.

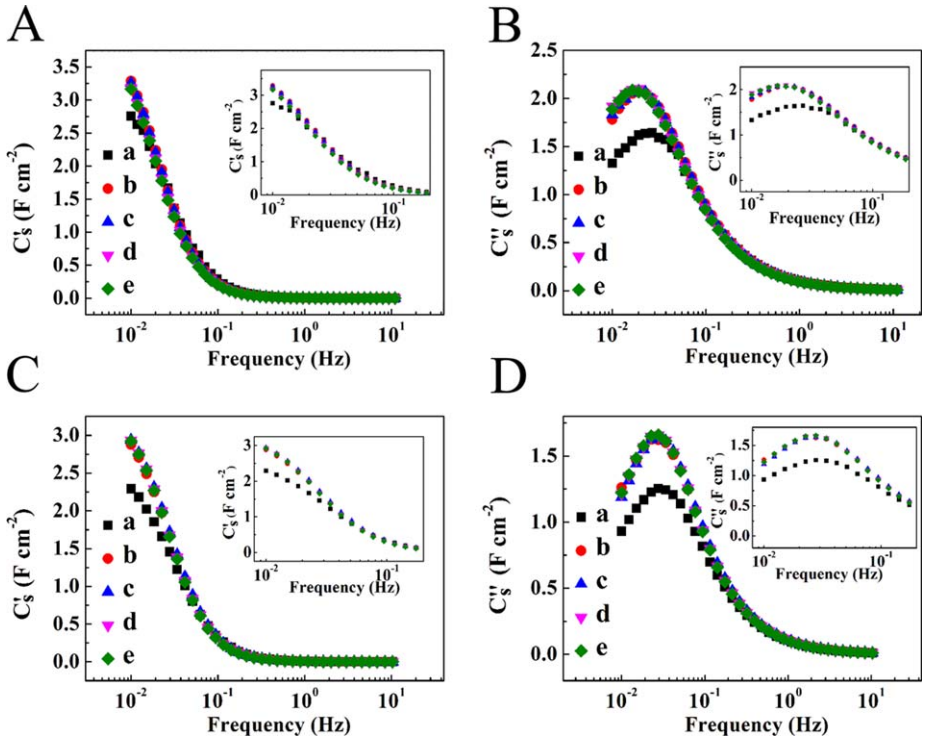

Figure 9. (A) C_s' and (B) C_s'' for Tiron-doped PPy and (C) C_s' and (D) C_s'' for Tiron-doped PPy/MWCNT composite with a mass of 27 mg cm^{-2} after (a) 1st, (b) 250th, (c) 500th, (d) 750th and (e) 1000th cycle, insets show low frequency range. [Color figure can be viewed in the online issue, which is available at wileyonlinelibrary.com.]

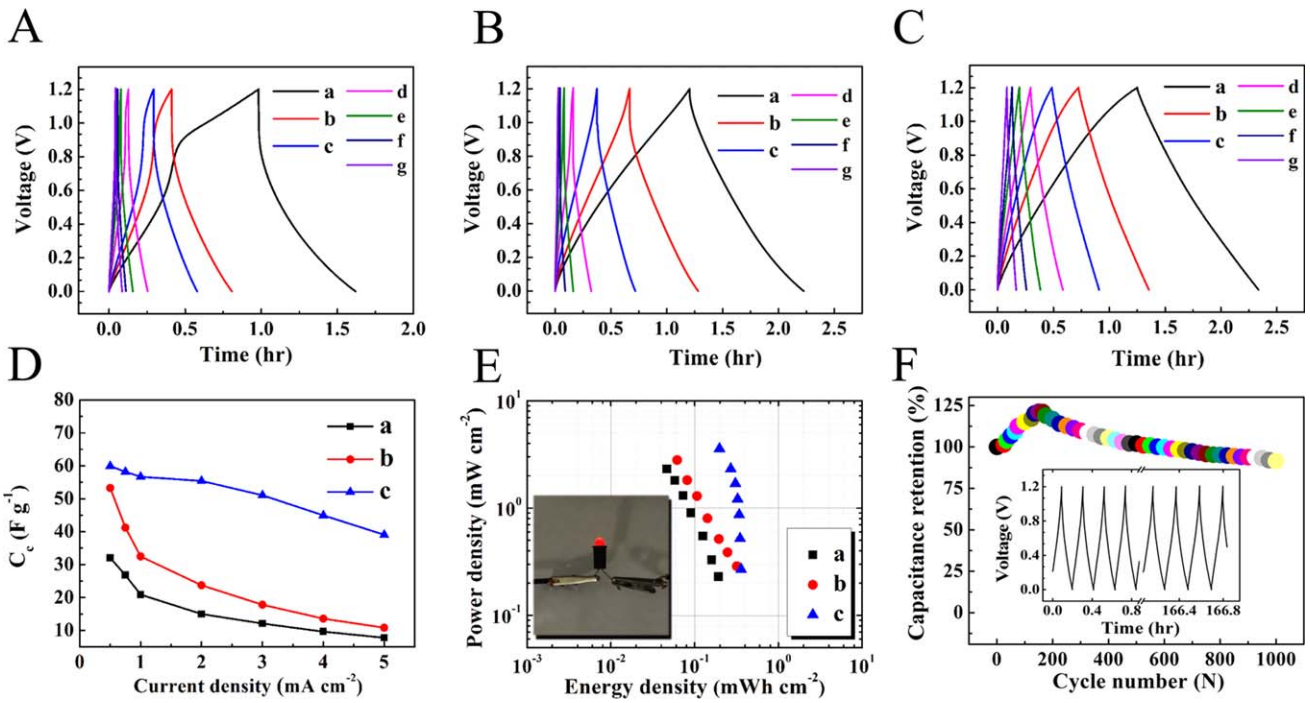

Figure 10. Galvanostatic charge–discharge curves of ES fabricated from (A) PPy without Tiron, (B) Tiron-doped PPy, and (C) Tiron-doped PPy/MWCNT composite at current densities: (a) 0.5, (b) 0.75, (c) 1, (d) 2, (e) 3, (f) 4, and (g) 5 mA cm^{-2}. (D) C_c versus current density obtained from the galvanostatic discharge data and (E) Ragone plot of the ES devices for (a) PPy without Tiron, (b) Tiron-doped PPy, and (c) Tiron-doped PPy/MWCNT composite (inset shows LED powered by a ES module). (F) Capacitance retention as a function of cycle number for Tiron-doped PPy/MWCNT composite ES, inset shows the charge/discharge curves at a constant current density of 5 mA cm^{-2} for the initial cycles and after 1000th cycle. [Color figure can be viewed in the online issue, which is available at wileyonlinelibrary.com.]

The capacitive performance of Tiron-doped PPy was studied during cycles using the impedance data [Figure 9(A–D)]. The real part of capacitance C′ decreased at frequencies above 0.1 Hz [shown in Figure 9(A,C)]. The corresponding dependence for the imaginary part C″ indicated the time constant τ of 36 s and 25 s for PPy without [Figure 9(B)] and with [Figure 9(D)] MWCNT, respectively. An increase of C* in the first 250 cycles was observed for both samples. The maxima in the frequency dependence of C″ shifted to slightly lower frequencies during cycling. These results confirmed good capacitive behavior and cycling stability of Tiron-doped PPy electrode with a high mass loading.

Finally we constructed symmetric ES devices with 15 mg on each electrode using different active materials. Galvanostatic charge/discharge properties of undoped PPy at different current densities are shown in Figure 10(A). Non-linear curves were observed for the PPy without dopant electrode. It was attributed to the limited contact area[54] between the conducting polymer and electrolyte due to agglomeration of PPy particles. The curves of the Tiron-doped PPy [Figure 10(B)] had nearly symmetrical triangular shape during the charge–discharge process at various current densities, which means that the Tiron-doped electrode exhibits better electrochemical capacitance performance compared with undoped PPy. However, the IR drop increased significantly with an increase in the current density. The Tiron-doped PPy/MWCNT composite ES shows a lower IR drop and longer charge–discharge times at the high current densities [Figure 10(C)]. C_c values calculated from the galvanostatic discharge data were plotted in Figure 10(D). The SC of Tiron-doped PPy symmetric supercapacitor is 54 F g^{-1} at a current density of 0.5 mA cm^{-2}, while the undoped PPy is only 32 F g^{-1}. However, as the scan rate increases to 5 mA cm^{-2}, C_c of Tiron-doped PPy sharply decreases to only 10 F g^{-1}. The PPy/MWCNT composite shows a SC of 60 F g^{-1} at a current density of 0.5 mA cm^{-2} and remains 39 F g^{-1} as the scan rate increases to 5 mA cm^{-2}. These results further prove that Tiron increases the SC of PPy and MWCNT and allows to improve the capacitance retention. The specific energy and specific power of the fabricated symmetric supercapacitor were estimated in the Ragone plot as shown in Figure 10(E). The maximum energy densities of undoped PPy and Tiron-doped PPy are 0.16 and 0.26 mWh cm^{-2}, respectively. Tiron-doped PPy without MWCNT revealed a significant decrease in specific energy with an increase of specific power. The specific energy values of Tiron-doped PPy/MWCNT composite electrode remained in the range of 0.20–0.34 mWh cm^{-2}, while the power density was in the range 0.52–3.68 mW cm^{-2}. The inset in Figure 10(E) shows LED bulbs with a nominal current of 20 mA, powered by the coin cells. Figure 10(F) shows cyclic behaviour of the symmetric supercapacitor and corresponding charge–discharge curves, which had similar triangular shape at the beginning and at the end of the cycling. The capacitance retention was found to be 91.4% after 1000 cycles. The increase in capacitance at the first 250 cycles can be attributed to the changes in the microstructure of the electrode material during cycling (Figure 8).

CONCLUSION

PPy has been synthesized by chemical polymerization using Tiron as dopant. SEM analysis indicated that Tiron reduced agglomeration and the particle size of PPy. The electrochemical tests demonstrated that at a scan rate of 0.5 mV s^{-1}, C_m of 180 F g^{-1} was obtained for undoped PPy electrode with a material loading of 14 mg cm^{-2}. Tiron allowed the improvement of charge storage of PPy, showing C_m of 310 F g^{-1}. SAF enabled the efficient dispersion of prepared PPy and MWCNT. FTIR data proved the adsorption of SAF molecules on PPy and MWCNT surface. The electron microscopy studies coupled with impedance spectroscopy measurements during cycling provided an insight into the cycle performance of Tiron-doped PPy and microstructure changes during cycling. The ES, prepared using PPy/MWCNT composite was able to deliver a maximum energy density of 0.36 mWh cm^{-2} and showed a good cycle stability with 91.4% capacitance retention after 1000 cycles.

ACKNOWLEDGMENTS

The authors gratefully acknowledge the Natural Sciences and Engineering Research Council of Canada for the financial support and Vale Canada Company for the donation of Ni foams.

REFERENCES

1. Snook, G. A.; Kao, P.; Best, A. S. *J. Power Sources* **2011**, *196*, 1.
2. Liu, J.; Li, M.; Zhang, Y.; Yang, L.; Yao, J. *J. Appl. Polym. Sci.* **2013**, *129*, 3787.
3. Liu, F.; Han, G.; Chang, Y.; Fu, D.; Li, Y.; Li, M. *J. Appl. Polym. Sci.* **2014**, *131*, 1097.
4. Liu, F.; Wang, S.; Han, G.; Liu, R.; Chang, Y.; Xiao, Y. *J. Appl. Polym. Sci.* **2014**, *131*, 1097.
5. Shi, K.; Zhitomirsky, I. *J. Mater. Chem. A* **2013**, *1*, 11614.
6. Shi, K.; Zhitomirsky, I. *J. Power Sources* **2013**, *240*, 42.
7. Pirvu, C.; Manole, C. C.; Stoian, A. B.; Demetrescu, I. *Electrochim. Acta* **2011**, *56*, 9893.
8. Zhang, G.; Zhou, H.; Zhang, J.; Han, X.; Chen, J.; Kuang, Y. *J. Appl. Polym. Sci.* **2012**, *125*, 2342.
9. Yu, Z.; Tetard, L.; Zhai, L.; Thomas, J. *Energy Environ. Sci.* **2015**, *8*, 702.
10. Yu, Z.; Li, C.; Abbitt, D.; Thomas, J. *J. Mater. Chem. A* **2014**, *2*, 10923.
11. Sultana, I.; Rahman, M. M.; Li, S.; Wang, J.; Wang, C.; Wallace, G. G.; Liu, H. *Electrochim. Acta* **2012**, *60*, 201.
12. Zeybek, B.; Pekmez, N. Ö.; Kılıç, E. *J. Appl. Polym. Sci.* **2014**, *131*, 1097.
13. Zhu, Y.; Shi, K.; Zhitomirsky, I. *J. Mater. Chem. A* **2014**, *2*, 14666.
14. Wang, P.; Yu, J. *React. Funct. Polym.* **2012**, *72*, 311.
15. Wang, Y.; Yang, C.; Liu, P. *Chem. Eng. J.* **2011**, *172*, 1137.
16. Feng, J.; Yan, W.; Zhang, L. *Microchim. Acta* **2009**, *166*, 261.
17. Yang, C.; Liu, P.; Zhao, Y. *Electrochim. Acta* **2010**, *55*, 6857.
18. Murray, P.; Spinks, G. M.; Wallace, G. G.; Burford, R. P. *Synth. Met.* **1997**, *84*, 847.

19. Mitchell, G. R.; Davis, F. J.; Legge, C. H. *Synth. Met.* **1988**, *26*, 247.
20. Lee, H.; Kim, H.; Cho, M. S.; Choi, J.; Lee, Y. *Electrochim. Acta* **2011**, *56*, 7460.
21. Lu, X.; Zhang, F.; Dou, H.; Yuan, C.; Yang, S.; Hao, L.; Shen, L.; Zhang, L.; Zhang, X. *Electrochim. Acta* **2012**, *69*, 160.
22. Hu, Y.; Zhao, Y.; Li, Y.; Li, H.; Shao, H.; Qu, L. *Electrochim. Acta* **2012**, *66*, 279.
23. Taberna, P. L.; Simon, P.; Fauvarque, J. F. *J. Electrochem. Soc.* **2003**, *150*, A292.
24. Goel, S.; Mazumdar, N. A.; Gupta, A. *Polym. Adv. Technol.* **2010**, *21*, 205.
25. Han, M.; Chu, Y.; Han, D.; Liu, Y. *J. Colloid. Interf. Sci.* **2006**, *296*, 110.
26. Weng, B.; Shepherd, R.; Chen, J.; Wallace, G. G. *J. Mater. Chem.* **2011**, *21*, 1918.
27. Shi, K.; Zhitomirsky, I. *ACS Appl. Mater. Interfaces* **2013**, *5*, 13161.
28. Vaisman, L.; Wagner, H. D.; Marom, G. *Adv. Colloid. Interface* **2006**, *128–130*, 37.
29. Kim, S. W.; Kim, T.; Kim, Y. S.; Choi, H. S.; Lim, H. J.; Yang, S. J.; Park, C. R. *Carbon* **2012**, *50*, 3.
30. Xie, X.; Mai, Y.; Zhou, X. *Mater. Sci. Eng. R* **2005**, *49*, 89.
31. Sun, Y.; Ata, M. S.; Zhitomirsky, I. *J. Colloid. Interf. Sci.* **2012**, *369*, 395.
32. Sun, Y.; Wang, Y.; Zhitomirsky, I. *Colloid. Surf. A* **2013**, *418*, 131.
33. Shi, K.; Zhitomirsky, I. *J. Colloid. Interf. Sci.* **2013**, *407*, 474.
34. Ćirić-Marjanović, G.; Blinova, N. V.; Trchová, M.; Stejskal, J. *J. Phys. Chem. B* **2007**, *111*, 2188.
35. Curran, S. A.; Ellis, A. V.; Vijayaraghavan, A.; Ajayan, P. M. *J. Chem. Phys.* **2004**, *120*, 4886.
36. Ma, P. C.; Kim, J.; Tang, B. Z. *Carbon* **2006**, *44*, 3232.
37. Santos, L. R. B.; Chartier, T.; Pagnoux, C.; Baumard, J. F.; Santillii, C. V.; Pulcinelli, S. H.; Larbot, A. *J. Eur. Ceram. Soc.* **2004**, *24*, 3713.
38. Tourillon, G.; Garnier, F. *J. Phys. Chem.* **1983**, *87*, 2289.
39. Hsu, F.; Wu, T. *Synth. Met.* **2012**, *162*, 682.
40. Rodríguez, I.; Scharifker, B. R.; Mostany, J. *J. Electroanal. Chem.* **2000**, *491*, 117.
41. Gogotsi, Y.; Simon, P. *Science* **2011**, *334*, 917.
42. Shi, K.; Ren, M.; Zhitomirsky, I. *ACS Sustainable Chem. Eng.* **2014**, *2*, 1289.
43. Zhu, Y.; Shi, K.; Zhitomirsky, I. *J. Power Sources* **2014**, *268*, 233.
44. Rodríguez, I.; Scharifker, B. R.; Mostany, J. *J. Electroanal. Chem.* **2000**, *491*, 117.
45. Håkansson, E.; Lin, T.; Wang, H.; Kaynak, A. *Synth. Met.* **2006**, *156*, 1194.
46. Mitchell, G. R.; Davis, F. J.; Legge, C. H. *Synth. Met.* **1988**, *26*, 247.
47. Talaie, A.; Wallace, G. G. *Synth. Met* **1994**, *63*, 83.
48. Zhang, X.; Bai, *Langmuir* **2003**, *19*, 10703.
49. Ardizzone, S.; Fregonara, G.; Trasatti, S. *Electrochim. Acta* **1990**, *35*, 263.
50. Vogt, H. *Electrochim. Acta* **1994**, *39*, 1981.
51. Baronetto, D.; Krstajić, N.; Trasatti, S. *Electrochim. Acta* **1994**, *39*, 2359.
52. Yu, Z.; McInnis, M.; Calderon, J.; Seal, S.; Zhai, L.; Thomas, J. *Nano Energy* **2015**, *11*, 611.
53. Wang, T.; Kiebele, A.; Ma, J.; Mhaisalkar, S.; Gruner, G. *J. Electrochem. Soc.* **2011**, *158*, A1.
54. Kim, M. S.; Moon, J. H.; Yoo, P. J.; Park, J. H. *J. Electrochem. Soc.* **2012**, *159*, A1052.